

Article

# Comprehensive Study of Au Nano-Mesh as a Catalyst in the Fabrication of Silicon Nanowires Arrays by Metal-Assisted Chemical Etching

Shanshan Wang, Huan Liu and Jun Han \*

School of Optoelectronic Engineering, Xi'an Technological University, Xi'an 710021, China; wangshanshan@xatu.edu.cn (S.W.); liuhuan@xatu.edu.cn (H.L.)

\* Correspondence: hanjun513@xatu.edu.cn; Tel.: +86-29-8617-3178

Received: 5 December 2018; Accepted: 16 February 2019; Published: 25 February 2019



**Abstract:** Silicon nanowires (SiNWs) arrays have become one of low-dimensional structural nanomaterials for the preparation of high-performance optoelectronic devices with the advantages of highly efficient light trapping effect, carrier multiplication, and adjustable optical bandgap. The controlled growth of SiNWs determines their electrical and optical properties. The morphology of silicon nanowires fabricated by conventional metal-assisted chemical etching (MACE) involving the Ag-based etching process cannot be precisely controlled. Ultra-thin anodic aluminum oxide (AAO) is one of the new-pattern nanostructure assembly systems for the synthesis of nanomaterials. The synthesized nanostructure arrays can be tuned to exhibit different optical and electrical properties in a certain wavelength range by adjusting the AAO membrane parameters. In this paper, we demonstrate an ultra-thin Au nano-meshes array from a single hexagonal AAO membrane as a replication master instead of conventional Ag particles as etching catalyst. The extended ordered silicon nanowires arrays are fabricated by the selective chemical dissolution of nanoscale noble metal meshes that exhibit excellent anti-reflection performance in broadband wavelengths and a wide incidence angle.

**Keywords:** SiNWs; MACE; AAO; anti-reflection performance; synthesized nanostructure arrays

## 1. Introduction

An array of silicon nanowires (SiNWs) is composed of numerous silicon wires arranged in an order that is perpendicular to the Si substrate. It is widely used in various biosensors, photoelectric detectors, and renewable energy devices by means of its enhanced absorptivity of incident light in a wide spectrum.

Generally, according to the growth direction and corresponding physical and chemical process, the preparation methods for silicon nanowires can be classified into two groups: “bottom-up” strategy and “top-down” strategy.

In the bottom-up approach, the compounds of silicon are decomposed as molecules and atoms by high temperature. Afterwards, they are recombined with physical phase change as solid single crystalline silicon nanowires. This approach mainly includes vapor–liquid–solid (VLS) [1,2], oxide-assisted growth (OAG) [3], and supercritical fluid based vapor–liquid–solid formation (SFLS) [4,5]. With this approach, by adjusting the initial conditions, such as metal catalysts, silicon nanowires with diameter of nanometer to hundreds of nanometer and length from nanometer to micron can be prepared. However, the grown nanowires are usually disordered. Gösele et al. [6–8] successfully solved this problem with ultrathin anodic aluminum oxide (AAO) template. Their approach was to deposit Au in the holes of AAO template and use the hole to

restrict the growth direction of nanowires. Finally, ordered silicon nanowires were collected after removing the AAO template with acid solution. One issue with this approach was that Au would be soaked into silicon causing pollution in the chemical vapor deposition (CVD) process with a high temperature environment.

While, in the top-down approach, silicon nanowires are obtained by chemical or physical etching to reduce the bulk silicon along a specified direction. This method mainly includes reactive ion etching (RIE), metal-assisted chemical etching (MACE), and laser ablation. The diameter of nanowire prepared by this method ranges from the nanometer to hundreds of nanometers. In the past twenty years, MACE has been applied to fabricate silicon nanowires with its unique advantages. The first report about MACE was in 1997 [9]; Dimova et al. obtained porous silicon in a short time by soaking silicon substrate with a thin layer of deposited Al in a mixed solution. In 2002, Peng et al. reported preparing SiNWs arrays with a mixture of HF/HNO<sub>3</sub> [10]. Huang et al. have further developed the MACE method to produce silicon nanowires with more detailed metal catalysts [11–18] and then made a comprehensive review about MACE [19].

MACE, which belongs to anisotropic wet etching method, has drawn extensive attentions for the advantages of simple fabrication, low cost, and formation of a large area of silicon nanowires [20,21]. The silicon nanowires fabricated by MACE have ranging from 5 nm to hundreds of nanometers in diameter and hundreds of nanometers to a few microns in length [19].

However, the growth of silicon wires fabricated by the conventional MACE method is generally disordered. The individual silicon wire is prone to cluster with surrounding Si wires due to surface tension, which will greatly influence its photoelectric properties. AAO membranes [22,23] have been employed for fabricating versatile ultra-thin metal films because of adjustable pore diameter, pore depth, pore density, and the distance of interpore, which is generally used as a sacrificial template by selective chemical dissolution with sodium hydroxide or phosphoric acid solution. Our experimental method is mainly an oriented reduction of silicon substrate in combination with chemical wet etching. Due to the catalytic activity of precious metal, the positive holes that are produced by reduction of oxidant are diffused by means of metal nanoparticles and then injected underneath the Si wafer. Meanwhile, Si is oxidized to SiO<sub>2</sub> by positive holes and it forms soluble silicates under the effect of HF. With the continuous sinking of metal nanoparticles, silicon nanowires arrays are fabricated on the surface of Si substrate. The thickness and uniformity of Ag films on Si substrate are important for the final morphology of SiNWs. Previously, we fabricated orderly inclined silicon nanowires by changing the etching parameters at room temperature and then analyzed the surface morphology of nanowires. However, the SiNWs arrays with diameter and density cannot be accurately controlled because of the random distribution of Ag ions.

The AAO membranes with pore diameter that is in the range of dozens to hundreds of nanometers, and with uniform pore density, can be conveniently prepared by anodic aluminum oxide, which are suitable for the preparation of monodisperse arrays with uniform diameter and spacing at the nanometer level, taking advantage of chemical stability, high temperature resistance, insulation, and transparency in the visible and most of the infrared light regions. The ultra-thin metal nano-meshes arrays can be obtained by removing AAO through the post sequential experimental process.

In this approach, the ordered ultra-thin Au nano-meshes arrays were fabricated by self-ordered hexagonal porous AAO membrane. The Au films can be used not only as a catalyst in the metal-assisted chemical etching, but also as a lithographic film for the pattern of the substrate [24].

Mostly, the AAO template is used as a sacrificial layer for Ag to control the structure and shape of the Ag mesh. There are many references on the synthesis of silicon nanowires with the catalysts of Ag particles and Ag mesh, but seldom used Au, except for Huang et al. [17,19]. They may be the first in using Au nano-mesh as a catalyst, however they have not detailed a comparative analysis of Au versus Ag.

However, the activity of Ag can cause secondary etching and produce excess positive holes. It is found that the Ag films at a higher temperature or extension of etching time will be dissolved and

cause taper shape with different diameters at the top and the bottom part and rough surface of the SiNWs. In addition, the chemical properties of Ag are relatively more active when compared with Au. Au is relatively stable, which can effectively suppress secondary etching and prevent undesired structural disintegration of ultra-thin metal films at elevated temperature. Besides, Au does not react with oxygen at high temperature.

In this paper, the properties of the silicon nanowires which were produced by combining Au instead of Ag with the AAO membrane as the sacrificial layer were detailed investigated.

## 2. Experiment

### 2.1. Pretreatment of Si Wafers

As substrate material,  $650 \pm 20 \mu\text{m}$  in thickness, resistivity ( $1\text{--}10 \Omega\cdot\text{cm}$ ) n-type,  $150 \pm 0.4 \text{ mm}$  in diameter,  $\langle 100 \rangle$  surface oriented single polished silicon chips are used in the experiment. The Si chips should be cleaned with  $\text{CH}_3\text{COCH}_3$ ,  $\text{CH}_3\text{CH}_2\text{OH}$ , and 5% HF solution in turn, and every clean step requires 5 min of ultrasonic vibration to remove the residual metal particles, organic contamination, and natural oxide layer on the surface of Si. These contaminations exist between the Au films and Si chips in the form of thin films or nanoparticles, which affect the second etching step, resulting in various defects with the sample morphology. Note here that AAO is an alumina film, which needs to be gently cut back and forth with a tailoring knife, otherwise it will be easily fractured.

### 2.2. Deposition of Au

The Au films with ordered arrays are deposited on the surface of AAO by ion sputter coater (SBC-12, KYKY Technology, Beijing, China). The sputtered Au films should not be too thin ( $<5 \text{ nm}$ ) or too thick ( $>25 \text{ nm}$ ). It is because the tension of solution will make the too thin ( $<5 \text{ nm}$ ) Au films that are completely damaged during the dissolution of AAO [25]. Too thick ( $>25 \text{ nm}$ ) Au films can hardly to be precipitated in the process of solution etching. Considering the above effects, we select four sets of sputtering parameters after repeated experiments to ensure integrated and delicate properties of the metal thin film, as depicted in Table 1.

**Table 1.** Four sets of sputtering parameters and film thickness.

Sputtering Current	Sputtering Time	Number of Sputtering	Thickness
3 mA	110 s	1	5.98 nm
3 mA	110 s	2	14.55 nm
3 mA	110 s	3	18.39 nm
3 mA	110 s	4	25.91 nm

### 2.3. Removal of AAO

Next, the AAO membranes that need to be removed as sacrificial layers provide the Si wafers with ordered metal nano-meshes array as growth templates for silicon wires [18]. Therefore, the Au films are separated from the AAO membranes by selective etching in sodium hydroxide solution for about 10 min at ambient temperature. The aluminum oxide is gradually dissolved by chemical reaction with sodium hydroxide, while the separated Au films remain afloat on the surface of the sodium hydroxide solution.

### 2.4. Transferring of Patterned Au films

Subsequently, the nanometer-sized Au films are transferred onto the pretreated Si substrate. The Au films are dried naturally to keep its integrity and smoothness. After drying, the Au films are attached to the Si wafers.

A Hitachi scanning electron microscope (SEM, SU1510, Hitachi, Tokyo, Japan) is employed to observe the microstructural characterization of the experimental samples. The SEM images of the Au

films attached to Si wafers are shown in Figure 1. It is observed that an average nano-hole size of Au mesh is a little smaller than that of the AAO membrane used for replication.

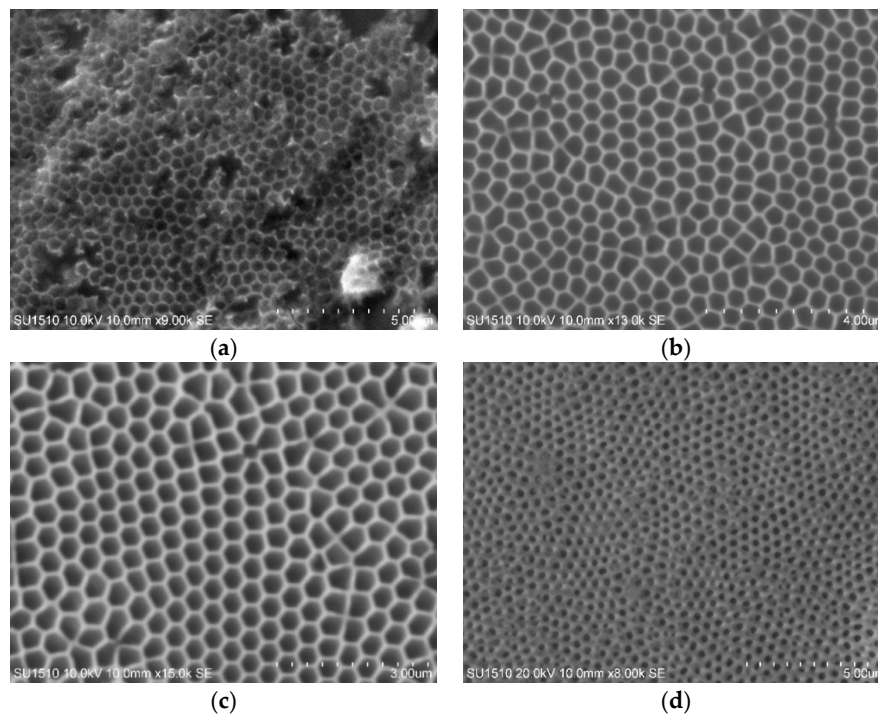


**Figure 1.** The scanning electron microscope (SEM) images of Au films that are obtained by replicating the ultrathin anodic aluminum oxide (AAO) mask, while the mask has been dissolved with NaOH solution as a sacrificial layer before SEM images are taken: (a) sputtering current: 3 mA; sputtering time: 110 s; the number of sputtering: 1; the thickness of Au mesh: 5.98 nm; (b) sputtering current: 3 mA; sputtering time: 110 s; the number of sputtering: 2; the thickness of Au mesh: 14.55 nm; (c) sputtering current: 3 mA; sputtering time: 110 s; the number of sputtering: 3; the thickness of Au mesh: 18.39 nm; and (d) sputtering current: 3 mA; sputtering time: 110 s; the number of sputtering: 4; the thickness of Au mesh: 25.91 nm.

As seen from Figure 1, no matter how many times of sputtering, the Au films are always conformal with the AAO membranes that present a hexagonal ordered array of nano-pores. The Au film sputtering for one time with thickness of about 6 nm and some areas have been damaged due to the tension of sodium hydroxide solution. After sputtering two or three times with thicknesses of about 15 and 18 nm, the Au meshes exhibit an integrate array pattern of AAO and the single mesh spacing is a moderately about 0.39  $\mu\text{m}$ . After four times of sputtering where thickness is about 25 nm, the Au meshes show better smoothness and integrity, but the side width of nano-meshes become larger and the single-mesh spacing is obviously less than 0.3  $\mu\text{m}$ , resulting in Au meshes with higher hardness. The Au films are not delicate enough to precipitate during the etching process. Another possible reason is the closure effect [17] of the pores of the metal films as the deposition proceeds, which leads to the gradual reduction of pores size. Ultimately, there are some pores that have diameters small enough to be sealed by the metal deposition. The closed pores are obviously unable to grow silicon nanowires. The thickness of metal meshes, which are closely related to the final morphologies of silicon nanowires, are proportional to sputtering time, sputtering current, and the times of sputtering.

### 2.5. Metal-Assisted Chemical Etching (MACE)

We performed MACE of the Si substrates that are coated with Au films immersed into a mixed etching solution of HF (40 wt %),  $\text{H}_2\text{O}_2$  (30 wt %) and  $\text{H}_2\text{O}$  at room temperature for about 50 min. The samples with sputtering one and four times do not form SiNWs arrays. While the sample with

sputtering two times forms an ordered silicon nanowires array with uniform diameter and density, and each silicon wire is independent from the others, without forming clusters. The nano-meshes of the sample with sputtering three times is blocked by metal particles and the silicon nanowires do not completely grow from the bottom to the top of the Au meshes.

### 3. Experiment Results

For comparison, the SEM images of SiNWs fabricated by conventional MACE with  $\text{AgNO}_3$  solution are displayed in Figure 2a, and the morphology of SiNWs fabricated by AAO membranes is shown in Figure 2b.

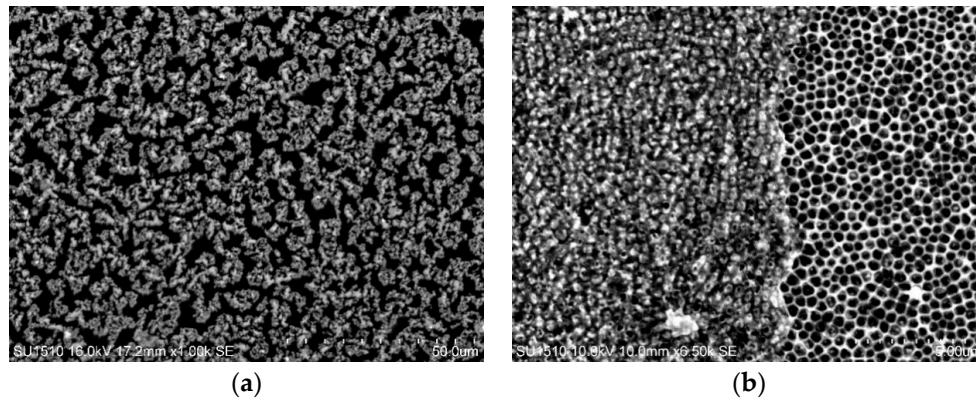


**Figure 2.** Comparison of SEM images of Silicon nanowires (SiNWs) fabricated by two methods: (a) the SiNWs fabricated by conventional MACE with  $\text{AgNO}_3$  solution; (b) the SiNWs fabricated with Au mesh replicated by AAO membrane.

It is observed in Figure 3 that the silicon nanowires that were fabricated by AAO membrane are not clustered into bundles. The silicon wires are about  $7\ \mu\text{m}$  in length and  $350\ \text{nm}$  in diameter. In the top view, many large holes appear on the surface of silicon wires arrays and the overall distribution is not uniform. On contrary, silicon nanowires that are fabricated by the AAO membrane reach the controllability of diameter and spacing and the overall distribution is uniform in Figure 4a. Figure 4b displays that the etching morphologies of area covered by Au films are in sharp contrast to the area not covered by Au films.

In our approach, the Au membranes not only act as a catalyst during the chemical etching, but they also provide photolithographic films for the patterns of Si substrate [26]. The conventional MACE is to form Ag films by immersing silicon wafer into  $\text{AgNO}_3$  solution. However, it is found that the Ag films at a higher temperatures or extension of etching time will be dissolved and cause structural damage, resulting in the rough surface of the SiNWs. In addition, the chemical properties of Ag are relatively more active when compared with Au, giving rise to the production of excessive positive holes, some of which are used for etching Si substrate and the excess diffuse to the top or lateral area of silicon wires. The secondary etching probably occurs under the effect of diffused positive holes. Therefore, we can see from the SEM image that there are small pores on the hexagon cylinder surface of silicon wires. The optical properties of SiNWs arrays do not reach the desired effect.

However, the chemical properties of Au are relatively stable, which can effectively suppress secondary etching and prevent the undesired structural disintegration of ultra-thin metal films at elevated experimental temperature. Huang et al. [14,27] reported that the SiNWs (aspect ratio = ca. 5) fabricated by using patterned silver membranes have tapered morphologies with different diameters at the top and the bottom part. This was mainly attributed to the decomposition of silver inducing a gradual increase of the meshes sizes in the process of etching with a certain period. Gold reacts with other elements to lose electrons in the outermost and sub-outermost layers. This process needs to absorb a lot of energy, which will inevitably increase its internal energy. Besides, gold is the

substance that does not react with oxygen at high temperature. This experiment verifies that the extended ordered SiNWs that were fabricated by using Au meshes arrays can attain the controllability of morphology, overcoming some of the disadvantages that are involved in conventional MACE with Ag ions as catalysts.

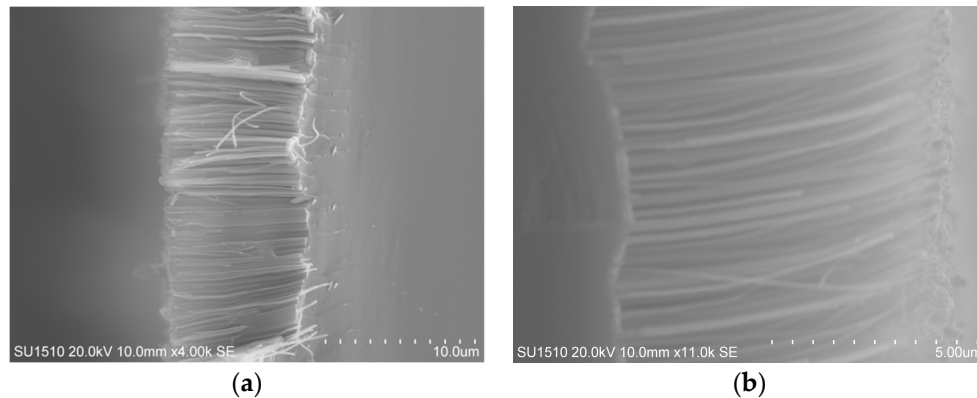


**Figure 3.** The SEM cross-sectional images of SiNWs fabricated by an AAO membrane at different magnification: (a)  $\times 4k$ ; (b)  $\times 11k$ .

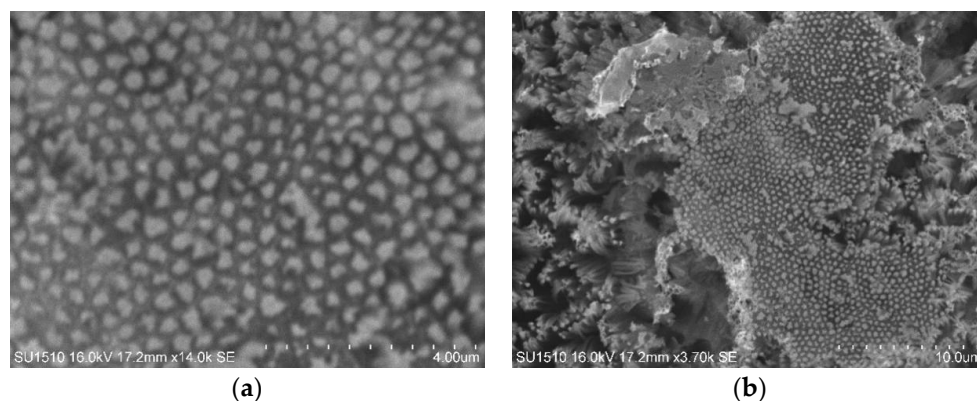


**Figure 4.** The SEM images of SiNWs fabricated by an AAO membrane, with the sputtering parameters (current is 3 mA, duration of sputtering is 110 s, 2 times of sputtering, thickness is 14.55 nm): (a) the local diagram of SiNWs; (b) large area diagram of SiNWs.

#### 4. Discussion

The hollow channel in the AAO membrane limits the growth direction of one-dimensional nanowires and the channel size controls the diameter of nanowires. The influence of the experimental parameters on the structure of SiNWs arrays has been verified in the previous section, and we need to further study the impact of the morphologies on silicon nanowires on the optical properties in depth. The entire transmittance and reflectivity in a wavelength ranging from visible to near infrared were measured by PerkinElmer UV/Vis/NIR Spectrometer equipped with an integrating sphere (Lambda950, PerkinElmer, Waltham, MA, USA). Figure 5 shows the comparison of transmittance and the reflectivity of the four different treated-samples as a function of wavelength.

As is depicted in Figure 5a, the light transmittance of the four samples is zero in the visible band (400–780 nm). The SiNWs that were fabricated by MACE with Ag as a catalyst can generate the lower transmittance in the range of near-infrared spectral regions. The red line is nearly 10% higher than the green and purple line, but over 20% lower than the polished Si chip. When the wavelength exceeds 1000 nm, the transmittance of four samples increase with an increase in the wavelength. The transmittance of the polished Si chip in the range of 1000–1200 nm increases by 40%, while the red line also increases by 20%. However, the green and purple lines only just increase by an average

10%. It can be seen from the measurement results in Figure 5a that the samples that were fabricated by controlled etching assisted with the ordered ultra-thin Au films replicated by AAO membranes have better performance on transmittance reduction in the near-infrared band range.

As shown in Figure 5b, the SiNWs that were fabricated by AAO membranes still have excellent performance on anti-reflection enhancement. It demonstrates that the three samples that have formed nanowires silicon arrays maintain a low reflective of average of 10% from visible light to near-infrared 1000 nm. When the wavelength exceeds 1050 nm, the reflectivity of all four samples increase with the increasing of wavelength. Nevertheless, the green and purple lines just still have low reflectivity in the near infrared, with 30% up to 1200 nm. Meanwhile, the reflectivity of red line increases sharply, which is close to that of the polished Si chip, at 55%. This is probably due to the random distribution of Ag ions and the excessive positive holes that are generated during the etching process affecting the overall morphology of SiNWs arrays. Nevertheless, the red line has a competitively low reflectivity at the wavelength range below 1050 nm, even lower than green line (the best morphology) by 5%, which indicates that it can be applied to other fields, such as solar cell.

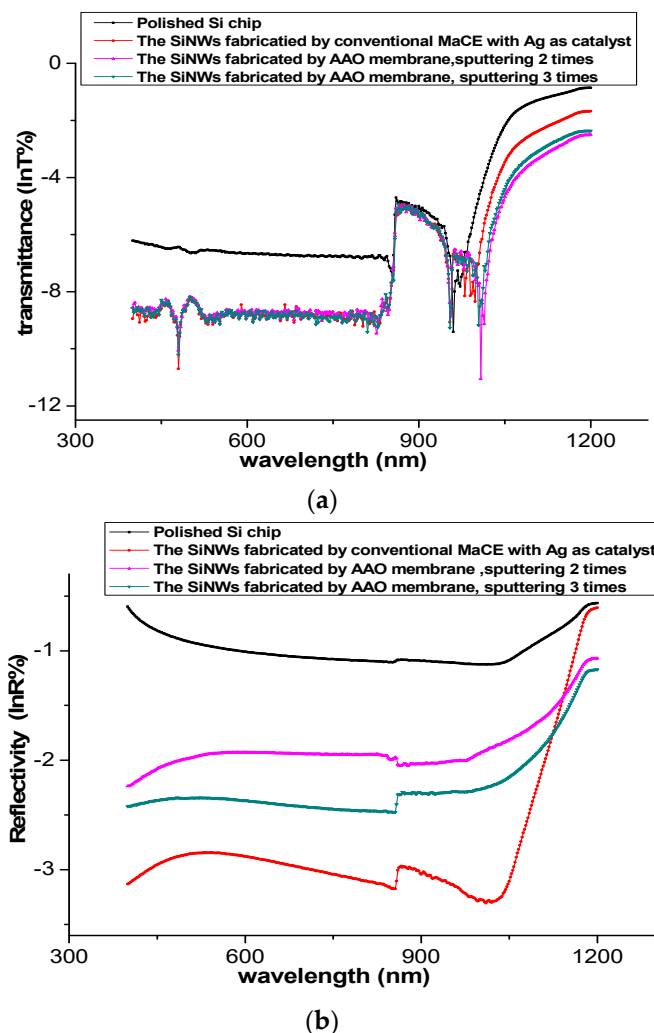


**Figure 5.** The comparison of optical properties of four different treated-samples: (a) the comparison of transmittance for four samples at different wavelengths; (b) the comparison of reflectivity of four samples at different wavelengths.

It is evident that the optical properties of SiNWs that were fabricated by AAO membranes are significantly superior to both of the compared samples. Large areas of uniform forest morphologies [28] that were prepared by controlled etching assisted with the ordered ultra-thin Au mesh replicated by the AAO membrane can both absorb the light, especially in the near-infrared band effectively, and improve the quantum efficiency. The average reflectivity of silicon nanowires arrays that were prepared with AAO membrane can be reduced to less than 18% in the whole visible and near-infrared bands. The unique forest structure of SiNWs arrays, which leads to multiple scattering of incident light inside, can enhance the antireflection effect. The arrays are capable of extracting light that is emitted in any direction of the array plane in order to improve the overall external efficiency [29]. The surface reflectivity of one-dimensional nanomaterial directly affects the photoelectric conversion efficiency of the detector [30,31]. The research on the controllability of SiNWs has not only important theoretical value, but also potential application prospect.

The researchers [32,33] believed that the enhanced light absorption characteristics of SiNWs arrays were probably caused by the strong resonance of incident light waves between the large scale uniformly aligned SiNWs on the surface of the monocrystalline silicon. Garnett and Yang [34] demonstrated that the ordered arrays of SiNWs increased the path length of incident solar radiation by up to a factor of 73. The extraordinary light-trapping path length enhancement factor was above the randomized scattering limit and it was superior to other light-trapping methods. They confirmed the array of vertical nanowires trapped incident light and led to an increase in the absorption for silicon solar cells, which can significantly benefit from increasing effective path length.

Peng et al. [35] proposed the micro-electrochemical mechanism for the growth of the silicon nanowires and proved that the preparation of SiNWs by MACE can effectively suppress the surface reflectivity and increase the light-trapping effect in broadband spectrum.

The Martin group [36] studied the physical structure of Au nano-films and the optical characteristics of AAO arrays system. The plasma resonance absorption band varied with the shape of Au nano-films. The size effect of Au films that were replicated by AAO nano-structured materials can realize the continuous adjustment of a visible region to control the selective absorption of light at a specific wavelength.

The Korea Research Institute of Standards and Science (KRISS) fabricated ordered arrays of silicon nanowires with noble metal meshes being replicated by ultrathin anodic aluminum oxide and explored a phenomenological model that explained the evolution of the morphology within the framework of the reaction kinetics [37,38]. They put forward a viewpoint by repeated experiments that the etching direction was mainly dictated by the etching rating. From the perspective of etching kinetics, the overall etching rate would be governed by the interplay between the injection of holes ( $h^+$ ) into silicon chips through the metal-silicon quasi-Schottky interface and the removal of oxidized silicon by HF from just underneath the noble metal catalyst. In this paper, we also obtained the experimental parameters of the uniform morphology of ordered silicon nanowires, which was closely related to the concentration of HF and  $H_2O_2$ . Therefore, the concentration of HF determined the generation of positive holes and the concentration of  $H_2O_2$  limited the removal of oxidized silicon [39,40].

Dutta et al. [41] prepared silicon nanowires arrays on n-type silicon substrates by metal-assisted chemical etching, depositing a layer of p-type silicon film on the surface to form PN junctions, and the structure of solar cells was obtained by spinning the nano-silicon particles on silicon films. The conversion efficiency of solar cells with this structure was much higher than that of ordinary amorphous silicon thin film solar cells. This also made use of the low reflectivity of the forest structure to achieve a high photoelectric conversion efficiency. Atwater and Polman [42] proposed the thin-film solar cells, with film thickness in the range 1–2  $\mu\text{m}$ , which can be deposited on cheap module-sized substrates, such as glass. The incident light would pass several times through the semiconductor film, resulting in the effective path length. The light can be concentrated and folded into the thin semiconductor layer, thereby increasing the absorption.

## 5. Conclusions

In this paper, the ultra-thin Au films with ordered nano-meshes arrays are prepared by sputtering AAO membranes. They are transferred to the n-type Si chips by the chemical method, and finally the extended arrays of SiNWs with controllable growth are fabricated on the surface of monocrystalline silicon by metal-assisted chemical wet etching. This method not only keeps the advantages of low cost and simple preparation, but it also avoids the random distribution of noble metal particles in conventional MACE, resulting in the uneven diameter and distribution density of silicon nanowires. The tests show that the average reflectivity of a sample fabricated by AAO membrane is about 20% lower than that obtained by conventional MACE in the visible and near-infrared wave band. The ordered forest structure, having exceptional anti-reflection, improves the conversion efficiency of photoelectric detectors and the meshes size of noble metal can be changed with the AAO membrane to expand the spectrum absorption range of incident light. Our result reveals that the controllable growth of silicon nanowires arrays has significant contribution in obtaining a high performance photoelectric detector.

**Author Contributions:** Conceptualization, S.W. and H.L.; Funding Acquisition, J.H.; Investigation, S.W. and H.L.; Methodology, S.W.; Project Administration, J.H.; Resources, S.W. and J.H.; Supervision, J.H.; Validation, S.W. and H.L.; Writing—Original Draft, S.W.; Writing—Review & Editing, S.W. and H.L.

**Funding:** This work was funded by the Xi'an Key Laboratory of Intelligent Detection and Perception (No. 201805061ZD12CG45).

**Acknowledgments:** We acknowledge the support from the key Laboratory Program of Shaanxi Province.

**Conflicts of Interest:** The authors declare no conflict of interest, and funders agree with the decision to publish the results.

## References

1. Renard, V.T.; Jublot, M.; Gergaud, P.; Cherns, P.; Rouchon, D.; Chabli, A.; Jousseau, V. Catalyst preparation for CMOS-compatible silicon nanowire synthesis. *Nat. Nanotechnol.* **2009**, *4*, 654–657. [[CrossRef](#)] [[PubMed](#)]
2. Wu, Y.; Cui, Y.; Huynh, L.; Barrelet, C.J.; Bell, D.C.; Lieber, C.M. Controlled growth and structures of molecular-scale silicon nanowires. *Nano Lett.* **2004**, *4*, 433–436. [[CrossRef](#)]
3. Shi, W.S.; Peng, H.Y.; Zheng, Y.F.; Wang, N.; Shang, N.G.; Pan, Z.W.; Lee, C.S.; Lee, S.T. Synthesis of large areas of highly oriented, very long silicon nanowires. *Adv. Mater.* **2000**, *12*, 1343–1345. [[CrossRef](#)]
4. Holmes, J.D.; Johnston, K.P.; Doty, R.C.; Korgel, B.A. Control of thickness and orientation of solution-grown silicon nanowires. *Science* **2000**, *287*, 1471–1473. [[CrossRef](#)] [[PubMed](#)]
5. Heitsch, A.T.; Fanfair, D.D.; Tuan, H.Y.; Korgel, B.A. Solution–liquid–solid (SLS) growth of silicon nanowires. *J. Am. Chem. Soc.* **2008**, *130*, 5436–5437. [[CrossRef](#)] [[PubMed](#)]
6. Shimizu, T.; Xie, T.; Nishikawa, J.; Shingubara, S.; Senz, S.; Gösele, U. Synthesis of vertical high-density epitaxial Si(100) nanowire arrays on a Si(100) substrate using an anodic aluminum oxide template. *Adv. Mater.* **2007**, *19*, 917–920. [[CrossRef](#)]
7. Zhang, Z.; Shimizu, T.; Senz, S.; Gösele, U. Ordered high-density Si(100) nanowire arrays epitaxially grown by bottom imprint method. *Adv. Mater.* **2009**, *21*, 2824–2828. [[CrossRef](#)]
8. Zhang, Z.; Shimizu, T.; Chen, L.; Senz, S.; Gösele, U. Bottom-imprint method for VSS growth of epitaxial silicon nanowire arrays with an aluminium catalyst. *Adv. Mater.* **2009**, *21*, 4701–4705. [[CrossRef](#)]
9. Diamova-Malinovska, D.; Sendova-Vassileva, M.; Tzenov, N.; Kamenova, M. Preparation of thin porous silicon layers by stain etching. *Thin Solid Films* **1997**, *297*, 9–12. [[CrossRef](#)]
10. Peng, K.Q.; Yan, Y.J.; Gao, S.P.; Zhu, J. Synthesis of large-area silicon nanowire arrays via self-assembling nanoelectrochemistry. *Adv. Mater.* **2002**, *14*, 1164–1167. [[CrossRef](#)]
11. Huang, Z.; Zhong, P.; Wang, C.; Zhang, X.; Zhang, C. Silicon nanowires/reduced graphene oxide composites for enhanced photoelectrochemical properties. *ACS Appl. Mater. Interfaces* **2013**, *5*, 1961–1966. [[CrossRef](#)] [[PubMed](#)]

12. Huang, Z.; Wang, R.; Jia, D.; Li, M.; Humphrey, M.G.; Zhang, C. Low-cost, large-scale, and facile production of Si nanowires exhibiting enhanced third-order optical nonlinearity. *ACS Appl. Mater. Interfaces* **2012**, *4*, 1553–1559. [[CrossRef](#)] [[PubMed](#)]
13. Huang, Z.; Liu, L.; Geyer, N. Quasi-radial growth of metal tube on Si nanowires template. *Nanoscale Res. Lett.* **2011**, *6*, 165. [[CrossRef](#)] [[PubMed](#)]
14. Huang, Z.; Shimizu, T.; Senz, S.; Zhang, Z.; Geyer, N.; Gösele, U. Oxidation rate effect on the direction of metal-assisted chemical and electrochemical etching of silicon. *J. Phys. Chem. C* **2010**, *114*, 10683–10690. [[CrossRef](#)]
15. Huang, Z.P.; Geyer, N.; Liu, L.F.; Li, M.Y.; Zhong, P. Metal-assisted electrochemical etching of silicon. *Nanotechnology* **2010**, *21*, 465301. [[CrossRef](#)] [[PubMed](#)]
16. Huang, Z.; Shimizu, T.; Senz, S.; Zhang, Z.; Zhang, X.; Lee, W.; Buczek, N.; Gösele, U. Ordered arrays of vertically aligned [110] silicon nanowires by suppressing the crystallographically preferred etching directions. *Nano Lett.* **2009**, *9*, 2519–2525. [[CrossRef](#)] [[PubMed](#)]
17. Huang, Z.; Zhang, X.; Reiche, M.; Liu, L.; Lee, W.; Shimizu, T.; Senz, S.; Gösele, U. Extended arrays of vertically aligned sub-10 nm diameter [100] Si nanowires by metal-assisted chemical etching. *Nano Lett.* **2008**, *8*, 3046–3051. [[CrossRef](#)] [[PubMed](#)]
18. Huang, Z.; Fang, H.; Zhu, J. Fabrication of silicon nanowire arrays with controlled diameter, length, and density. *Adv. Mater.* **2007**, *19*, 744–748. [[CrossRef](#)]
19. Huang, Z.; Geyer, N.; Werner, P.; de Boor, J.; Gösele, U. Metal-assisted chemical etching of silicon: A review. *Adv. Mater.* **2011**, *23*, 285–308. [[CrossRef](#)] [[PubMed](#)]
20. Sun, L.; Fan, Y.; Wang, X.; Susantyoko, R.A.; Zhang, Q. Large scale low cost fabrication of diameter controllable silicon nanowire arrays. *Nanotechnology* **2014**, *25*, 255302. [[CrossRef](#)] [[PubMed](#)]
21. Peng, K.; Lu, A.; Zhang, R.; Lee, S.T. Motility of metal nanoparticles in silicon and induced anisotropic silicon etching. *Adv. Funct. Mater.* **2008**, *18*, 3026–3035. [[CrossRef](#)]
22. Zhang, J.L.; Hong, G.Y. The nanomaterials synthesized by using AAO template. *Chin. J. Appl. Chem.* **2004**, *21*, 6–11.
23. Whitesides, G.M.; Grzybowski, B. Self-assembly at all scales. *Science* **2002**, *295*, 2418–2421. [[CrossRef](#)] [[PubMed](#)]
24. Park, S.J.; Han, H.; Rhu, H.; Baik, S.; Lee, W. A versatile ultra-thin Au nanomesh from a reusable anodic aluminum of oxide (AAO) membrane. *J. Mater. Chem. C* **2013**, *1*, 5330–5335. [[CrossRef](#)]
25. Homma, T. Fabrication of nanostructured functional thin films through wet processes (technology for magnetic film fabrication II). *J. Magn. Soc. Jpn.* **2005**, *29*, 1035–1040. (In Japanese)
26. Juhasz, R.; Elfstrom, N.; Linnros, J. Controlled fabrication of silicon nanowires by electron beam lithography and electrochemical size reduction. *Nano Lett.* **2005**, *5*, 275–280. [[CrossRef](#)] [[PubMed](#)]
27. Peng, K.; Zhang, M.; Lu, A.; Wong, N.B.; Zhang, R.; Lee, S.T. Ordered silicon nanowire arrays via nanosphere lithography and metal-induced etching. *Appl. Phys. Lett.* **2007**, *90*, 85. [[CrossRef](#)]
28. Niu, L.; Jiang, X.; Zhao, Y.; Ma, H.; Yang, J.; Cheng, K.; Du, Z. Large-area, size-tunable Si nanopillar arrays with enhanced antireflective and plasmonic properties. *Nanotechnology* **2016**, *27*, 315601. [[CrossRef](#)] [[PubMed](#)]
29. Pecora, E.F.; Lawrence, N.; Gregg, P.; Trevino, J.; Artoni, P.; Irrera, A.; Priolo, F.; Dal Negro, L. Nanopatterning of silicon nanowires for enhancing visible photoluminescence. *Nanoscale* **2012**, *4*, 2863–2866. [[CrossRef](#)] [[PubMed](#)]
30. Kim, H.; Zhang, A.; Cheng, J.; Lo, Y.H. High sensitivity visible and IR (1550 nm) Si nanowire photodetectors. In *Quantum Sensing and Nanophotonic Devices VII, Proceedings of the SPIE OPTO, San Francisco, CA, USA, 23–28 January 2010*; Rzeghi, M., Sudharsanan, R., Brown, G.J., Eds.; SPIE: Bellingham, WA, USA, 2010; pp. 169–185.
31. Kelzenberg, M.D.; Boettcher, S.W.; Petykiewicz, J.A.; Turner-Evans, D.B.; Putnam, M.C.; Warren, E.L.; Spurgeon, J.M.; Briggs, R.M.; Lewis, N.S.; Atwater, H.A. Enhanced absorption and carrier collection in Si wire arrays for photovoltaic applications. *Nat. Mater.* **2010**, *9*, 239–244. [[CrossRef](#)] [[PubMed](#)]
32. Sivakov, V.; Andrä, G.; Gawlik, A.; Berger, A.; Plentz, J.; Falk, F.; Christiansen, S.H. Silicon nanowire-based solar cells on glass: Synthesis, optical properties and cell parameters. *Nano Lett.* **2009**, *9*, 1549–1554. [[CrossRef](#)] [[PubMed](#)]

33. Tsakalakos, L.; Balch, J.E.; Fronheiser, J.; Shih, M.Y.; LeBoeuf, S.F.; Pietrzykowski, M.; Codella, P.J.; Korevaar, B.A.; Sulima, O.; Rand, J.; et al. Strong broadband optical absorption in silicon nanowire films. *J. Nanophotonics* **2007**, *1*, 165–182. [[CrossRef](#)]
34. Garnett, E.; Yang, P.D. Light trapping in silicon nanowire solar cells. *Nano Lett.* **2010**, *10*, 1082–1087. [[CrossRef](#)] [[PubMed](#)]
35. Peng, K.; Xu, Y.; Wu, Y.; Yan, Y.; Lee, S.T.; Zhu, J. Aligned single-crystalline Si nanowire arrays for photovoltaic applications. *Small* **2010**, *1*, 1062–1067. [[CrossRef](#)] [[PubMed](#)]
36. Hulteen, J.C.; Martin, C.R. A general template-based method for the preparation of nanomaterials. *J. Mater. Chem.* **1997**, *7*, 1075–1087. [[CrossRef](#)]
37. Kim, J.; Han, H.; Kim, Y.H.; Choi, S.H.; Kim, J.C.; Lee, W. Au/Ag bilayered metal mesh as a Si etching catalyst for controlled fabrication of Si nanowires. *ACS Nano* **2011**, *5*, 3222–3229. [[CrossRef](#)] [[PubMed](#)]
38. Mounni, B.; Jaballah, A.B. Correlation between oxidant concentrations, morphological aspects and etching kinetics of silicon nanowires during silver-assist electroless etching. *Appl. Surf. Sci.* **2017**, *425*, 1–7. [[CrossRef](#)]
39. Li, X.; Bohn, P.W. Metal-assisted chemical etching in HF/H<sub>2</sub>O<sub>2</sub> produces porous silicon. *Appl. Phys. Lett.* **2000**, *77*, 2572–2574. [[CrossRef](#)]
40. Chen, C.-Y.; Wu, C.-S.; Chou, C.-J.; Yen, T.-J. Morphological control of single-crystalline silicon nanowire arrays near room temperature. *Adv. Mater.* **2010**, *20*, 3811–3815. [[CrossRef](#)]
41. Gu, Q.; Dang, H.; Cao, J.; Zhao, J.; Fan, S. Silicon nanowires grown on iron-patterned silicon substrates. *Appl. Phys. Lett.* **2000**, *76*, 3020–3021. [[CrossRef](#)]
42. Atwater, H.A.; Polman, A. Plasmonics for improved photovoltaic devices. *Nat. Mater.* **2010**, *3*, 205–213. [[CrossRef](#)] [[PubMed](#)]



© 2019 by the authors. Licensee MDPI, Basel, Switzerland. This article is an open access article distributed under the terms and conditions of the Creative Commons Attribution (CC BY) license (<http://creativecommons.org/licenses/by/4.0/>).